Direct Torque Control Scheme for a Six-Phase Induction Motor with Reduced Torque Ripple

Jay K. Pandit, *Student Member*, *IEEE*, Mohan V. Aware, *Senior Member*, *IEEE*,
Ronak Nemade, *Student Member*, *IEEE*, Emil Levi, *Fellow*, *IEEE*

***Abstract*–This paper presents an improved direct torque control (DTC) method for an asymmetrical six-phase induction motor using a two-level six-phase inverter. As is well-known, a simple extension of three-phase direct torque control technique to an asymmetrical six-phase motor, using large vectors only, introduces significant current harmonics of the order $6n\pm1$ (n = 1,3,5,…), which are mapped into the non-flux/torque producing (xy) plane. These harmonics cause only losses in the motor winding as they do not take part in torque production. Hence a number of different improved DTC techniques have been developed in the past for multiphase motor drives. The paper takes one such DTC method as the starting point and improves it further by using the concept of virtual voltage vectors. Developed vector selection algorithm, based on two virtual voltage vectors, requires the information on position of the flux in the auxiliary (xy) subspace and provides stator current quality commensurate with the currently available best DTC algorithm for six-phase drives. However, use of two virtual voltage vectors enables a substantial reduction of the torque ripple, which is achieved by means of a five-level torque comparator. Extensive experimentation is performed and it is shown that the reduction of the current harmonics is in essence almost the same as in another recently developed DTC scheme, based on the use of a single virtual voltage vector. However, the achieved torque ripple reduction, which is verified experimentally, makes the scheme superior when compared to the existing approaches. At the same time, developed scheme retains qualities of conventional DTC schemes, such as simple structure and fast response. Its additional beneficial feature is the easiness of implementation.**

***Index Terms*—Asymmetrical six-phase machines, Direct torque control, Induction machines, Torque ripple.**

NOMENCLATURE

L_{ls}, L_{lr}	Stator and rotor leakage inductances, respectively.
L_s, L_r	Self-inductances of stator and rotor, respectively.
L_m	Mutual inductance.
R_s	Stator resistance.
R_r	Rotor resistance.
v_{ds}, v_{qs}	dq subspace voltage.
v_{xs}, v_{ys}	xy subspace voltage.
ψ_{ds}, ψ_{qs}	dq subspace flux components.
ψ_{xs}, ψ_{ys}	xy subspace flux components.
P	Number of pole pairs.
T_e	Electromagnetic torque.
ΔT_e	Torque ripple.
ω_r	Rotor angular speed.

Manuscript received 15 July 2016; revised 19 September 2016; accepted 21 October 2016.

J. K. Pandit, M. V. Aware and R. Nemade are with the Dept. of Electrical Engineering, Visvesvaraya National Institute of Technology, Nagpur 440010, India (e-mail: jaypandit2007@gmail.com, mva_win@yahoo.com, rnemade11@gmail.com).

E. Levi is with the Faculty of Engineering and Technology, Liverpool John Moores University, Liverpool L3 3AF, UK (e-mail: e.levi@ljmu.ac.uk).

I. INTRODUCTION

Multi-phase machines, introduced in the 1960's, have come into the focus of attention in the electric drives area in recent times. The original reason for their investigation was the problem of the low-order torque ripple, generated by six-step operation of a three-phase inverter. For an n-phase machine the lowest order torque ripple producing current harmonics are of the order $2n\pm1$. Thus, taking as an example a five-phase machine, the lowest order harmonic torque ripple is produced by the 9th and 11th current harmonics and takes place at 10 times the fundamental frequency.

Multi-phase machines possess inherent advantages over the three-phase counterparts, such as better fault-tolerant characteristics, power/current splitting into a higher number of converter legs enabling reduction of the required semiconductor rating, possibility of independent control of multiple motor drives using a single inverter, and suitability for designing fully-integrated on-board battery chargers for electric vehicles, as discussed in recent surveys [1]-[5]. The major application areas of multi-phase drives are a more-electric aircraft, ship propulsion, electric and hybrid electric vehicles, locomotive traction, and general high-power industrial applications [1]-[5]. Among the variety of multi-phase machine options, an asymmetrical six-phase machine is preferred since it can be easily obtained by rewinding the stator of a three-phase machine as long as the number of slots per pole per phase is an even number [6].

In an asymmetrical six-phase machine, with two-three-phase windings spatially shifted by 30°, the order of the torque ripple producing currents is given by $12n\pm1$ (n = 0,1,2,…), whereas currents of the order $6n\pm1$ (n = 1,3,5,…) do not contribute to either the average torque or torque ripple production [7]. They however produce losses and reduce the drive efficiency since there is no back-emf for the harmonic currents of the order $6n\pm1$, and the impedance seen by these harmonic currents comprises winding resistance and stator leakage inductance only. Thus, for relatively small magnitudes of voltage harmonics of the order $6n\pm1$ (n = 1,3,5…), harmonic currents of substantial magnitudes result.

Direct Torque Control (DTC) emerged as an alternative to vector control for three-phase ac drives and is characterised with a simple structure, fast torque response and robustness

against machine parameter variations [8], [9]. The problem of harmonic current reduction is addressed for a variety of DTC schemes for asymmetrical six-phase (dual three-phase, split phase) drives in [10]–[13]. Harmonic current reduction is achieved by individual flux control technique in [10]. In [11], a deadbeat DTC technique is proposed to reduce current harmonics and improve drive response by achieving constant switching frequency. A modified lookup table based DTC technique is developed for reduction of current harmonics in [12]. In the modified lookup table based DTC technique selection of the voltage vector depends on the position of flux in the auxiliary (*xy*) subspace. DTC is also considered for five-phase machines in [14], [15]. A virtual voltage vector technique, which is similar to the modified lookup table based technique, is proposed in [15], where the problem of flux reduction at low speeds is also addressed.

A concept of synthetic voltage vector was introduced in [13] and [14] for dual-three phase and five-phase machines, respectively. Employment of synthetic vectors eliminates the need for stator flux position estimation in the auxiliary *xy* subspace. Investigations of torque ripple reduction techniques for a six-phase machine are available in [10] and [16]. Paper [10] proposes individual flux control technique and modified torque comparator for achieving harmonic current reduction and torque ripple reduction, respectively. Strategy proposed in [16] aims to reduce current harmonics and torque ripple by using synthetic voltage vectors and a multilevel torque comparator.

A possibility of employing virtual voltage vectors for torque ripple reduction has not been investigated in literature for asymmetrical six-phase machines and this is the subject this paper deals with. While the approach using two virtual voltage vectors, developed in this paper, shares some similarities with [16], where two synthetic voltage vectors were used, there are important differences that make the approach of this paper superior. In particular, neither the design of a switching sequence nor the use of PWM modulators are required. Next, as a single virtual vector is applied during the whole sampling time period, the average switching frequency is reduced. This automatically means that, due to the lower switching losses, the inverter operation will be more efficient. The virtual voltage vector selection procedure requires estimation of the flux position in the auxiliary subspace; however, this does not involve any additional hardware, since motor phase currents are measured anyway.

The paper is organized as follows. Section II summarizes the model of an asymmetrical six-phase induction motor, based on the Vector Space Decomposition (VSD) technique. A six-phase two-level voltage source inverter and the mapping of the inverter voltage space vectors into different subspaces are also briefly revisited in section II. Extension of the classical DTC to an asymmetrical six-phase induction motor, based on large vectors only, is reviewed in section III. Section IV presents a modified DTC technique for a six-phase inverter, which focuses on the auxiliary subspace current component reduction. Use of the virtual vector concept to simultaneously reduce the auxiliary subspace current components and the torque ripple, using two virtual voltage vectors and a five-level torque comparator, is described in section V. Experimental studies are conducted on a laboratory drive system for all three considered DTC techniques and comparative experimental results are presented in section VI. Conclusions of the investigation are summarized in section VII.

II. Motor and Inverter Models

A. Asymmetrical Six-Phase Motor Model

An asymmetrical six-phase induction motor has two sets of stator three-phase windings, which are displaced spatially by 30° (electrical). The VSD technique, developed in [7], is used to model the motor. It transforms a six-dimensional system into a set of three two-dimensional mutually orthogonal subspaces (*dq*, *xy* and $0_1 0_2$). The transformation matrix is given with [7]:

$$[T]=\frac{1}{3}\begin{bmatrix} 1 & \cos\pi/6 & \cos 4\pi/6 & \cos 5\pi/6 & \cos 8\pi/6 & \cos 9\pi/6 \\ 0 & \sin\pi/6 & \sin 4\pi/6 & \sin 5\pi/6 & \sin 8\pi/6 & \sin 9\pi/6 \\ 1 & \cos 5\pi/6 & \cos 8\pi/6 & \cos\pi/6 & \cos 4\pi/6 & \cos 9\pi/6 \\ 0 & \sin 5\pi/6 & \sin 8\pi/6 & \sin\pi/6 & \sin 4\pi/6 & \sin 9\pi/6 \\ 1 & 0 & 1 & 0 & 1 & 0 \\ 0 & 1 & 0 & 1 & 0 & 1 \end{bmatrix} \tag{1}$$

The transformation matrix (1) maps the fundamental components and the harmonics of the order $12n\pm1$ (n = 1,2,3,…) into the *dq* subspace, while harmonics of the order $6n\pm1$ (n = 1,3,5,…) are mapped into the *xy* subspace. Harmonics of the order $3n$ (n = 1,3,5…) are mapped into the $0_1 0_2$ subspace. Only the current harmonics of the *dq* subspace lead to the torque production in a machine with near-sinusoidal magneto-motive force distribution (this is the type of the machine considered here).

The motor is modelled in the stationary reference frame. Application of (1) to the stator and rotor voltage/flux equations of the phase-variable motor model and subsequent application of the rotational transformation in conjunction with the rotor winding lead to the motor model, which is given with:

$$\begin{aligned} v_{ds} &= R_s i_{ds} + d\psi_{ds}/dt \\ v_{qs} &= R_s i_{qs} + d\psi_{qs}/dt \\ v_{xs} &= R_s i_{xs} + L_{ls} di_{xs}/dt \\ v_{ys} &= R_s i_{ys} + L_{ls} di_{ys}/dt \end{aligned} \tag{2}$$

$$\begin{aligned} 0 &= R_r i_{dr} + d\psi_{dr}/dt + \omega_r \psi_{qr} \\ 0 &= R_r i_{qr} + d\psi_{qr}/dt - \omega_r \psi_{dr} \end{aligned} \tag{3}$$

$$\begin{aligned} \psi_{ds} &= (L_{ls}+L_m) i_{ds} + L_m i_{dr} \\ \psi_{qs} &= (L_{ls}+L_m) i_{qs} + L_m i_{qr} \\ \psi_{dr} &= (L_{ls}+L_m) i_{dr} + L_m i_{ds} \\ \psi_{qr} &= (L_{ls}+L_m) i_{qr} + L_m i_{qs} \\ \psi_{xs} &= L_{ls} i_{xs} \\ \psi_{ys} &= L_{ls} i_{ys} \end{aligned} \tag{4}$$

$$T_e = 3P\left(\psi_{ds} i_{qs} - \psi_{qs} i_{ds}\right) \tag{5}$$

Equations for zero-sequence $0_1 0_2$ components are omitted since the machine is considered as having two isolated neutral points (Fig. 1), so that the flow of zero-sequence current is not possible.

B. Six-Phase Two-Level Inverter

Two three-phase two level Voltage Source Inverters (VSIs) with common dc source are used to realise a six-phase VSI. Each inverter leg can be in one of the two switching states, depending on whether the upper or the lower switch is on (S = 1 or 0, respectively). For a six-phase inverter, there are $2^6 = 64$ possible switching combinations. Each switching combination is defined by a binary value of $V_i = S_a S_b S_c S_d S_e S_f$, where S_x ($x = a, b, c, d, e, f$) is the switching function of the corresponding leg and V_i is the voltage vector formed by the i^{th} switching combination. Every vector generated by the six-phase VSI has particular projections in the *dq* and *xy* subspaces, which can be obtained using [7] ($a = \exp(j\pi/6)$):

$$V_{dq} = V_d + jV_q = \frac{1}{3}\left(V_a + aV_b + a^4V_c + a^5V_d + a^8V_e + a^9V_f\right)$$
$$V_{xy} = V_x + jV_y = \frac{1}{3}\left(V_a + a^5V_b + a^8V_c + aV_d + a^4V_e + a^9V_f\right) \quad (6)$$

All the 64 vectors are classified into two categories, active vectors (60 of them) and zero vectors (4 of them). Out of 60 active vectors, 12 vectors are redundant; hence there are 48 effective active vectors. Projections of all active space vectors in the *dq* and *xy* subspaces are shown in Fig. 2. The active vectors are grouped according to the descending order of their lengths (L_1, L_2, L_3, L_4). Hence, vectors of the group L_1 are the longest and those of L_4 are the shortest. Each group of vectors form a dodecagon when their tips are connected together with straight lines.

III. Classical DTC

Switching table based DTC of a three-phase induction motor drive can be extended to an asymmetrical six-phase induction motor drive with minor modifications in the lookup table (Fig. 3). With availability of more vectors, *dq* subspace is divided into 12 sectors, as shown in Fig. 4. In classical DTC (termed further on DTC1 for the sake of brevity), only active vectors from group L_1 are used and their impact on the *xy* subspace current harmonics is not considered. It is a well-known fact that this DTC scheme leads to large harmonic currents in the *xy* subspace and is therefore inadequate. The classic DTC is used here for the benchmarking purposes only.

In Fig. 3 phase voltages are estimated from the switching function and dc-bus voltage (V_{dc}) of the inverter. Voltages and currents in the *dq* subspace are obtained by transforming phase voltages and currents using (1). Stator flux components in the *dq* subspace are estimated using the voltage model (the first two equations of (2)) and torque is then estimated using (5). Stator flux magnitude is controlled by a two-level hysteresis flux comparator. Torque is controlled by a three-level hysteresis torque comparator. Position of the flux in the *dq* subspace is estimated using the estimated stator flux *dq* components, obtained from the voltage model.

Consider the stator flux vector ψ_s positioned in sector i, as shown in Fig. 4. Vectors which will increase torque are V_{60} and V_{28}, while the vectors which will decrease the torque are V_3 and V_{35}. The torque is maintained at the current level by applying zero vectors. Similarly, vectors V_{60} and V_{35} lead to an increase in the flux magnitude and vectors V_3 and V_{28} provide decrease in the flux magnitude. According to this discussion and the commands given by the flux and torque comparators, switching table is formulated and is given by Table I.

As discussed already, every vector has particular projections in both the *dq* and *xy* subspaces. DTC1 does not take into consideration behaviour of the applied voltage vectors in the *xy* subspace.

IV. Modified DTC

A modified switching table DTC for an asymmetrical six-phase Permanent Magnet Synchronous Motor (PMSM) was proposed in [12]. This DTC technique is referred to further on as 'modified DTC' technique and denoted simply as DTC2. By using DTC2, currents in the *xy* subspace are reduced, thus overcoming the main drawback of the DTC1. Block diagram of the DTC2 is given in Fig. 5. It utilises two different switching tables. The first one is the same as that of the DTC1 (Table II-a), while the second switching table is shown in Table II-b.

A. Reduction of xy Subspace Components

When flux lies in sector i and both flux and torque are to be increased, voltage vector V_{60} is selected from the switching table 1, whereas vector V_{24} is selected from the switching table 2 (Table II-a and II-b). In the *dq* subspace, vectors V_{60} and V_{24} are located at the same position and are hence in phase. Both vectors therefore have similar effect on the flux and torque behaviour. On the contrary, in the *xy* subspace, Fig. 2b shows that the vectors V_{60} and V_{24} are in phase opposition. Similar to the *dq* subspace, 12 sectors of the *xy* subspace are defined in Fig. 2b using notation i to xii. The *xy* subspace is divided into two semicircles C_1 and C_2, with the dividing line between them being perpendicular to the vectors V_{60} and V_{24} (Fig. 2b).

Position of the flux in the *xy* subspace is estimated by using the last two equations of (4). If the flux position is in the semicircle C_1, vector V_{24} is selected, while if the flux position is in the semicircle C_2, vector V_{60} is selected. In both cases resultant flux in the *xy* subspace will decrease, since the vector from the opposite semicircle is applied. This vector selection strategy is summarized in Table III. Switching tables II-a and II-b of Table II use active vectors from groups L_1 and L_2, respectively. Both tables receive the same inputs from the flux and torque comparators. Outputs of both tables are multi-

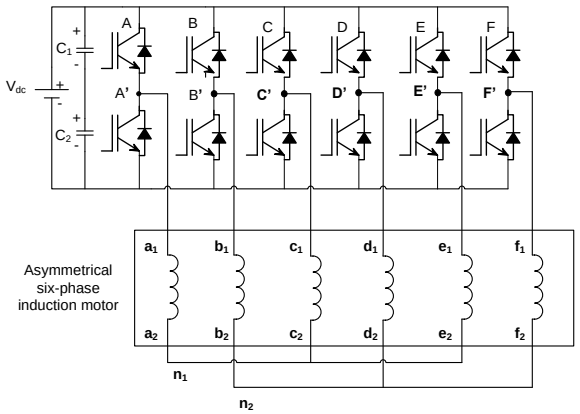

Fig. 1. Asymmetrical six-phase drive's configuration.

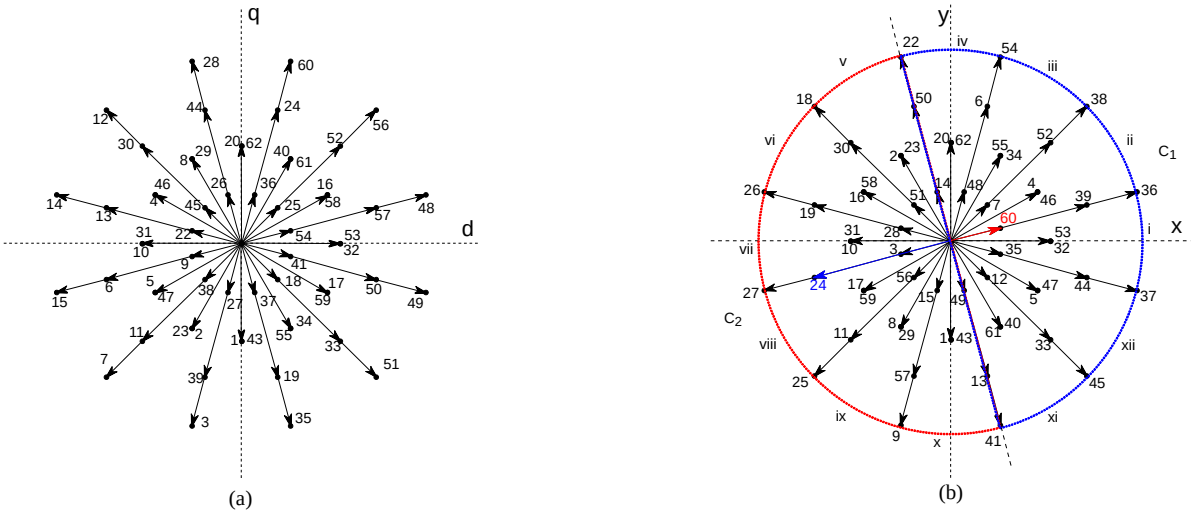

Fig. 2. Projections of voltage vectors in (a) *dq* subspace (b) *xy* subspace.

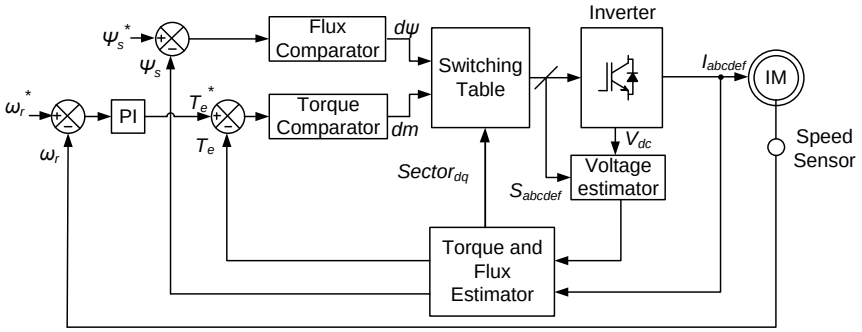

Fig. 3. Control scheme of the classical DTC (DTC1). Variables *dψ* and *dm* denote flux and torque commands, respectively.

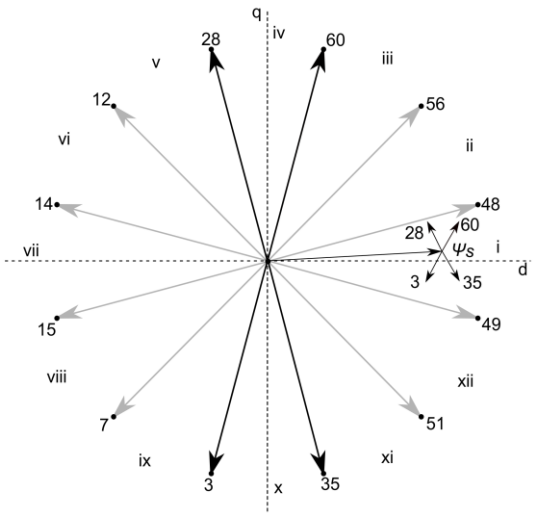

Fig. 4. Voltage vectors used in the DTC1 and their selection procedure.

plexed using 2:1 multiplexer. Vector selection between two vectors is decided by Table III. For example, let us assume that vectors V_{60} and V_{24} are selected by the switching tables given in Table II-a and Table II-b, respectively. With reference to Fig. 2b, if flux is located in the semicircle C_1 (from sector v to x of the *xy* subspace), then vector V_{24} is selected by Table III; if flux is located in the semicircle C_2 (from sector i to iv and sector xi to xii of the *xy* subspace), the vector V_{60} is selected by Table III. Table III gives the selection bit for the 2:1 multiplexer. If 1 is selected by the Table III, the vector selected from the switching table 1 (Table II-a) is supplied to the inverter, while, if 2 is selected by the Table III, the vector selected by the switching table 2 (Table II-b) is supplied to the inverter. At any point in time only one out of the two vectors would be supplied to the inverter. For the remaining vectors of the group L_1 Table III can be extended along the same lines.

TABLE I. SWITCHING TABLE FOR THE DTC1.

Sector i		*dm*		
		1	0	–1
dψ	1	V_{60}	V_0	V_{35}
	0	V_{28}	V_0	V_3

TABLE II. SWITCHING TABLES FOR DTC2, BASED ON [12].

a. Switching Table 1

Sector i		*dm*		
		1	0	–1
dψ	1	V_{60}	V_0	V_{35}
	0	V_{28}	V_0	V_3

b. Switching Table 2

Sector i		*dm*		
		1	0	–1
dψ	1	V_{24}	V_0	V_{19}
	0	V_{44}	V_0	V_{39}

V. PROPOSED DTC

Compared to the DTC1, DTC2 reduces the negative effects of the space vectors in the *xy* subspace. On the other hand, performance of the drive in terms of torque ripple is unchanged, since a three-level torque comparator is still used. An attempt is made here to reduce torque ripple by suggesting a different voltage vector selection principle for the DTC. While DTC2 uses two groups of vectors (L_1 and L_2), DTC proposed here (and labelled as DTC3) uses an additional combination of vectors (L_2 and L_4), similar to [16].

A. Reduction of xy Subspace Components

Consider vectors V_{60}, V_{24} and V_{36}. These three vectors are in phase with each other in the *dq* subspace, as can be seen in Fig. 2a. Hence all three vectors will have similar effect on the flux and torque changes. However, in the *xy* subspace vectors V_{60} and V_{36} are in phase, while vector V_{24} is in phase opposition with vectors V_{60} and V_{36}. An algorithm similar to the DTC2 is therefore formulated for the selection criterion between vectors V_{36} and V_{24}. Let us assume that vectors V_{36} and V_{24} are selected from the switching tables 1 and 2 analogous to Table II, respectively; then, depending on the position of the flux in the *xy* subspace, a vector selection needs to be done to decide whether V_{36} or V_{24} should be applied. As shown in Fig. 2b, if flux vector lies in the semicircle C_1 then vector V_{24} is selected, while if flux lies in the semicircle C_2 vector V_{36} is selected. Similarly, for vectors V_{60} and V_{24} selected from switching tables of Table II, respectively, if flux vector lies in the semicircle C_1 then V_{24} is selected; if the flux vector lies in the semicircle C_2 vector V_{60} is selected. The choice of vectors is such that it always tends to reduce the magnitude of the flux vector in the *xy* subspace.

Probability of selection of either V_{36} or V_{24} as a function of the position of the flux vector in the *xy* subspace is 50%. Similarly, probability of selection of either V_{60} or V_{24}, again depending on the position of the flux vector in the *xy* subspace, is also 50%. Combination of vectors V_{36} and V_{24} constitutes a virtual vector V_{S3} and combination of vectors V_{60} and V_{24} constitutes a virtual vector V_{L3}. The lengths of the virtual vector V_{S3} and V_{L3} are given with

$$|V_{S3}| = \frac{|V_{36}| + |V_{24}|}{2} = \frac{0.173V_{dc} + 0.471V_{dc}}{2} = 0.322V_{dc}$$
$$|V_{L3}| = \frac{|V_{60}| + |V_{24}|}{2} = \frac{0.644V_{dc} + 0.471V_{dc}}{2} = 0.5575V_{dc} \quad (7)$$

Virtual vector set V_{Sx} (x = 1,2…12) is constituted for combinations of vectors from groups L_2 and L_4. Virtual vector set V_{Lx} (x = 1,2…12) is formed for combinations of vectors from groups L_1 and L_2 and lengths of vectors V_{Sx} and V_{Lx} are given by (7). Projections of all virtual vectors in the *dq* subspace are shown in Fig. 6. There are 24 virtual vectors in total, use of which always tends to reduce the *xy* subspace components. The results on the right-hand side of equations (7) are the same for any pair of virtual vectors $|V_{Sx}|$, $|V_{Lx}|$ ($x = 1,2...12$) since the lenghts of all vectors within each individual vector group are the same.

B. Torque Slopes for Different Voltage Vectors

Torque slope equations for three-phase induction motor drive are derived in [17] and [18]. Equations are formulated along the same lines for an asymmetrical six-phase induction machine drive here, with the derivation being identical to the one in [17], [18] and with the only difference in the final result stemming from the different expression for the six-phase machine's torque (5), when compared to a three-phase machine. The rate of change of torque for utilization of active vectors and zero vectors, respectively, is therefore given with

$$S_1 = \frac{dT_e}{dt} = -\frac{T_e}{\sigma\tau_{sr}} + 3P\frac{L_m}{\sigma L_s L_r}\left[\left(v_{qs}\psi_{dr} - v_{ds}\psi_{qr}\right) - \omega_r\left(\psi_{ds}\psi_{dr} + \psi_{qs}\psi_{qr}\right)\right]$$
$$S_2 = \frac{dT_e}{dt} = -\frac{T_e}{\sigma\tau_{sr}} - 3P\frac{L_m}{\sigma L_s L_r}\omega_r\left(\psi_{ds}\psi_{dr} + \psi_{qs}\psi_{qr}\right) \quad (8)$$

where $\sigma = \left(1 - L_m^2\right)/\left(L_s L_r\right)$, $\sigma\tau_{sr} = \left(R_s/\sigma L_s + R_r/\sigma L_r\right)^{-1}$. It is clear from (8) that the rate of change of torque for active vectors is dependent on the magnitude of the voltage vector and motor speed. However, it follows from (8) that the zero vector always tends to reduce the torque and the rate of reduction is dependent on the motor speed. At lower speeds, the rate of reduction is slow, while for higher speeds the rate of reduction is fast. This behaviour is illustrated in Fig. 7 for the DTC1.

For vectors V_{Sx}, change in torque is positive at lower speeds and is negative at higher speeds. Change in torque for vectors V_{Lx} is positive for all speeds but the rate of rise depends on the speed of motor. For lower speeds torque rise due to V_{Lx} is steep, while it becomes gradual at higher speeds. Rate of rise of torque due to V_{Sx} is slower when compared to the rate of rise due to V_{Lx} for lower speeds, as the rate of rise depends on

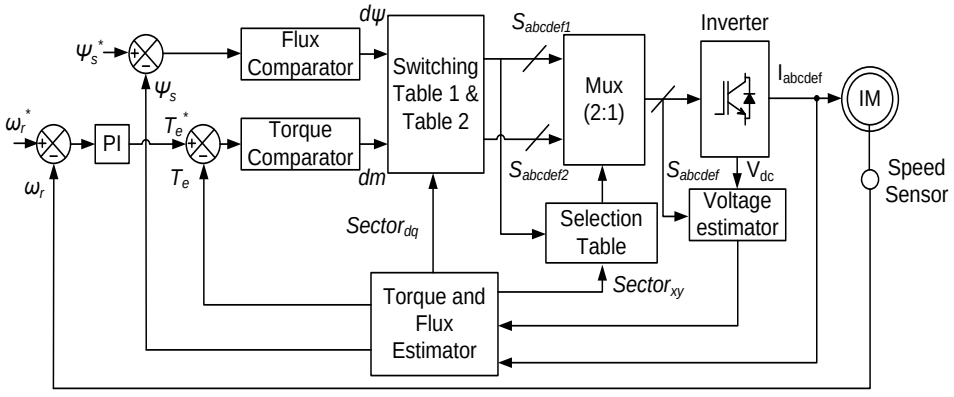

Fig. 5. Block diagram of the DTC2.

TABLE III. VECTOR SELECTION TABLE (1 AND 2 REFER TO SWITCHING TABLES 1 AND 2 OF TABLE II).

vector / sector$_{xy}$	i	ii	iii	iv	v	vi	vii	viii	ix	x	xi	xii
V_{60}	2	2	2	2	1	1	1	1	1	1	2	2

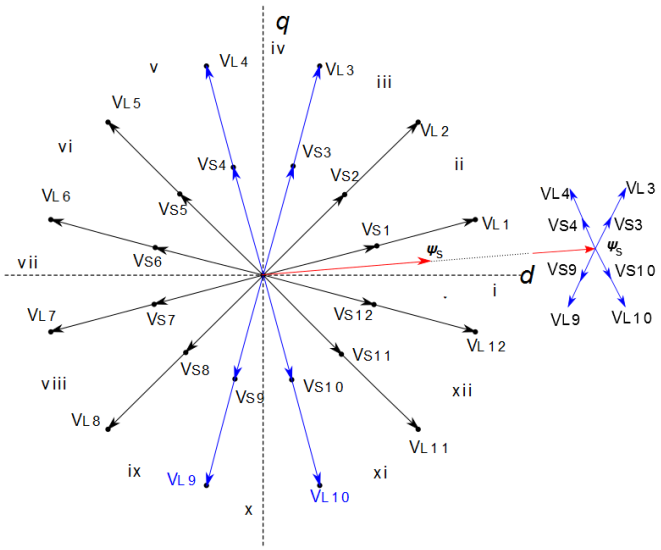

Fig. 6. Virtual vectors of DTC3 in the *dq* subspace.

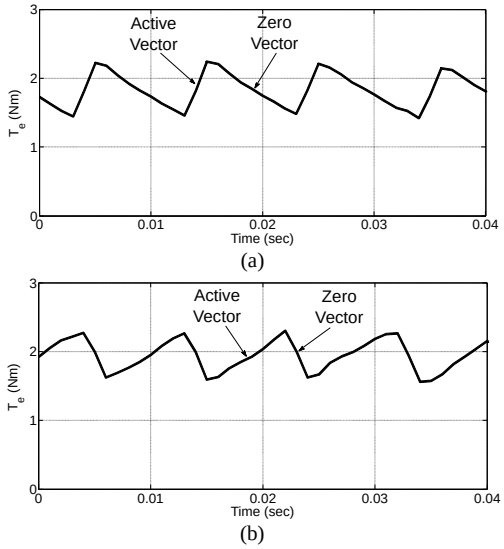

Fig. 7. Estimated electromagnetic torque behaviour at (a) 500 rpm, and (b) 2500 rpm for DTC1 (experimental results).

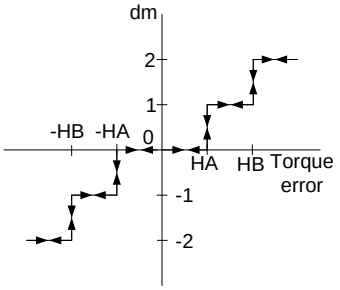

Fig. 8. A five-level torque comparator.

TABLE IV. SWITCHING TABLE FOR THE DTC3.

Sector i		*dm*				
		2	1	0	-1	-2
$d\psi$	1	V_{L3}	V_{S3}	V_0	V_{S10}	V_{L10}
	0	V_{L4}	V_{S4}	V_0	V_{S9}	V_{L9}

the magnitude of the voltage vector. For higher speeds, the rate of reduction of torque due to V_{Sx} is more gradual when compared to the one caused by the zero vector.

C. Torque Ripple Reduction

Multi-level torque comparator has been proposed in [15], [16], [18], [19] as a mean for torque ripple reduction. In DTC3 developed here, a five-level torque comparator, shown in Fig. 8, is used. When the torque error is greater than the HB, a torque command is given so as to increase torque rapidly.

When torque error is higher than HA but less than HB, a torque command is given so as to increase torque gradually. Vector V_{Lx} is used when a large rate of change is expected and vector V_{Sx} is used when a small rate of change is expected. The rate of change of torque is dependent on the magnitude of the vector selected. Hence the ratio of bandwidths of the torque comparators is equal to the ratio of the magnitudes of the respective vectors [16] and is given with

$$H_A : H_B = |V_{Sx}| : |V_{Lx}| = 0.322V_{dc} : 0.5575V_{dc} \quad (9)$$

At low speeds the rate of rise of torque due to active vectors is faster than the rate of fall due to the zero vector. On the contrary, at higher speeds the rate of fall of torque due to zero vectors is faster than the rate of rise due to the active vectors, as can be observed in Fig. 7. For reducing torque ripple, the steeper slopes (rate of rise of torque for lower speeds and rate of fall of torque at higher speeds) should be made more gradual. Vectors V_{Lx} and V_{Sx} provide positive torque slopes at lower speeds. The rate of rise of torque due to V_{Sx} is slower as compared to that of the rate of rise due to V_{Lx}. Hence, under steady state condition, at lower speeds V_{Sx} is used instead of V_{Lx} for torque ripple reduction. Higher speeds are achieved with the use of full length vectors. For higher speeds zero vector and V_{Sx} both provide negative torque slopes. The rate of fall of torque due to zero vector is steeper compared to the rate of fall due to V_{Sx}. Hence, under steady state condition, at higher speeds V_{Sx} is used instead of the zero vector for torque ripple reduction. Based on this discussion a new switching table, shown in Table IV, is formulated for the DTC3.

As discussed in [20], average torque under steady state condition is lower than the torque reference. Under steady state condition, V_{Sx} and zero vectors are used at low speeds; hence torque error is maintained between 0 and HA. For higher speeds, under steady state condition, vectors V_{Sx} and V_{Lx} are used, so that torque error is maintained between HA and HB. For all speeds in steady state operation torque error is not zero. This problem could be addressed by band shifting technique proposed in [20].

VI. EXPERIMENTAL RESULTS

Three DTC techniques, discussed in the previous sections, have been tested on the laboratory setup with a six-phase drive. Parameters of the asymmetrical six-phase motor are given in Table V. Control block diagrams of a six-phase machine with DTC1 and DTC2-DTC3 are shown in Fig. 3 and Fig. 5, respectively. Control algorithm, stator flux and torque

estimators, and the switching tables are incorporated in Digital Signal Processor (DSP) TMS320F28377S. Sampling frequency of 10 kHz is maintained in all tests. A 12-bit Digital to Analogue Converter (DAC) is available on-board TMS320F28377S. Estimated signals in digital form are converted to analogue signals using DACs. Estimated signals in analogue form are recorded using digital oscilloscope. Recorded signals are plotted with Matlab plotting tool.

A shaft encoder with a resolution of 1500 pulses per revolution (ppr) is used for speed measurement. An enhanced quadrature encoder pulse module, present in the DSP TMS320F28377S, is used for frequency measurement of pulses from encoder and for detection of the direction of rotation. An eddy current brake is used to provide mechanical loading. Experimental setup is shown in Fig. 9. In DTC3, torque bands HA and HB are set as 0.173Nm and 0.3Nm, respectively, and DTC3 is tested in both steady state and dynamic operation. For DTC1 and DTC2 the torque hysteresis band equals 0.3 Nm, while the flux hysteresis band is 0.003 Wb for all three DTC techniques. Also, performance of the proposed technique is compared with DTC1 and DTC2 for different loading and speed conditions.

TABLE V. MACHINE PARAMETERS.

Parameter	Value
Number of poles	2
Stator resistance	6 Ω
Rotor resistance	2.2 Ω
Stator leakage inductance	14.4 mH
Rotor leakage inductance	14.4 mH
Mutual inductance	256 mH
Rated power	0.75 kW
Dc link voltage	300 V

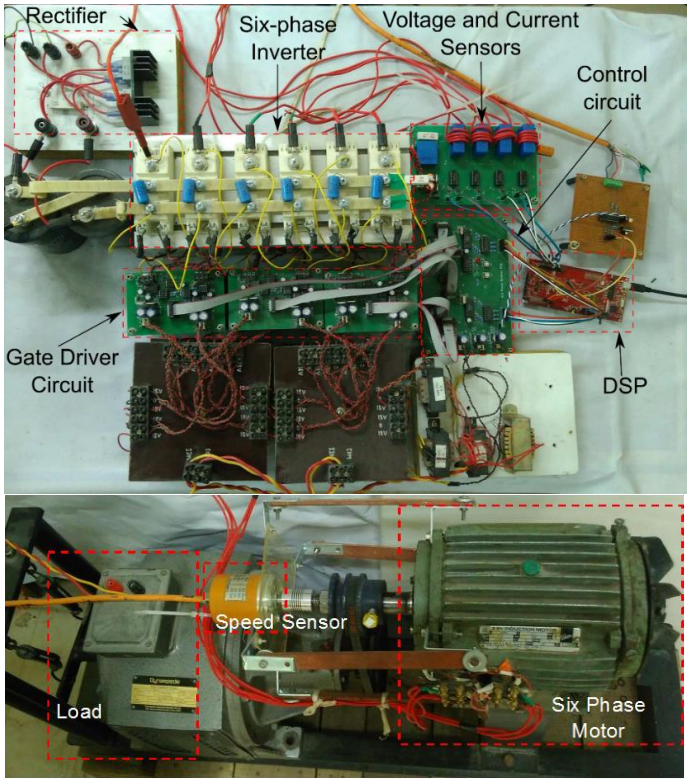

Fig. 9. Experimental setup.

Stator currents are measured using current sensors LA25-P. Flux estimation in the *dq* subspace, as noted already, uses reconstructed stator voltages and stator current measurement in conjunction with the stator voltage model. No filtering is applied and pure integrators are used. Flux position in the *xy* subspace is obtained using measured stator currents and stator leakage inductance. In the experimental results that follow torque traces are estimated torque waveforms. The drive operates with closed loop speed control at all times and a PI controller is used for this purpose.

A. Steady State Operation

In steady state condition motor is operated at 2500 rpm with 2 Nm loading. Figs. 10-12 show trajectory of the estimated flux in the *dq* and *xy* subspaces for DTC1, DTC2 and DTC3 techniques, respectively. Trajectory of flux in the *dq* subspace remains essentially the same for DTC3, when compared with DTC1 and DTC2. Fig. 10b shows the trajectory of flux in *xy* subspace for DTC1. Since the effect of voltage vectors in the *xy* subspace is not considered in DTC1, the flux trajectory shows substantial values. Fig. 11b shows the trajectory of the flux in the *xy* subspace for DTC2. Comparison of trajectories of flux in the *xy* subspace for DTC1 and DTC2 shows a substantial reduction of flux excursions in the *xy* subspace in the latter case, achieved by consideration of both subspaces in the process of voltage vector selection. Flux trajectory in the *xy* subspace for DTC3 is depicted in Fig. 12b. It is evident from comparison of Fig. 10b and Fig. 12b that the effect of voltage vectors in the *xy* subspace is significantly reduced with the DTC3 technique and that the flux trajectory shows the values that are insignificantly higher than with DTC2 (Fig. 11b).

Steady state currents of phases *a* and *b* and FFT analysis of the phase *a* current for the three studied DTC methods are shown in Fig. 13 for the same conditions as in Figs. 10-12. In addition to the fundamental component, harmonics of the order $6n\pm1$ (n = 1,3,5,…) appear, as can be seen from the plots of the spectra. These harmonics are of substantial values in the case of DTC1 (Fig. 13a), while both DTC2 and DTC3 reduce them significantly (Figs. 13b and 13c). It can be seen that the performance of the DTC3 is only insignificantly worse in this respect than the one offered by DTC2.

Variation in Total Harmonic Distortion (THD) of phase current with load is compared for the three DTC methods in Fig. 14 at three different operating speeds. Current THD is significantly higher, as expected, with DTC1, since the low order current harmonics $6n\pm1$ (n = 1,3,5,…) dominate the spectrum. Current THD for DTC2 and DTC3 is practically the same throughout the operating range of speeds and load torques, which validates reduction of the *xy* subspace components in DTC3 and confirms that the reduction is commensurate with the one achieved using DTC2.

Electromagnetic torque under steady state condition for the three DTC techniques is shown in Fig. 15. Load torque is once more 2 Nm and motor speed is 2500 rpm. Torque ripple is calculated using

$$\Delta T_e = \sqrt{\frac{1}{j}\sum_{i=1}^{j}\left(T_{ei} - T_{eave}\right)^2} \tag{9}$$

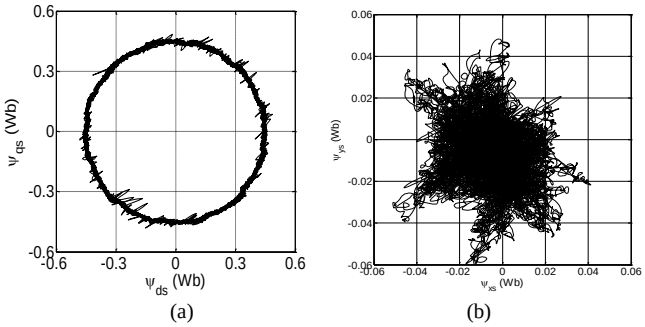

Fig. 10. Stator flux in (a) *dq* subspace and (b) *xy* subspace for DTC1.

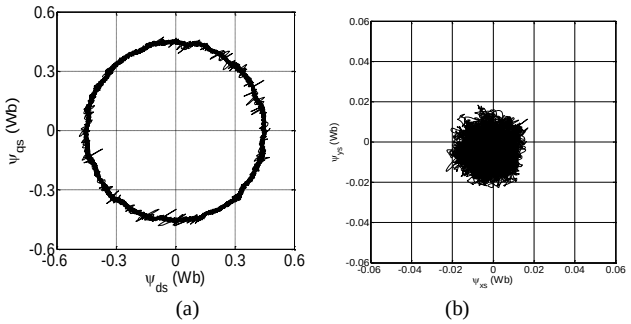

Fig. 11. Stator flux in (a) *dq* subspace and (b) *xy* subspace for DTC2.

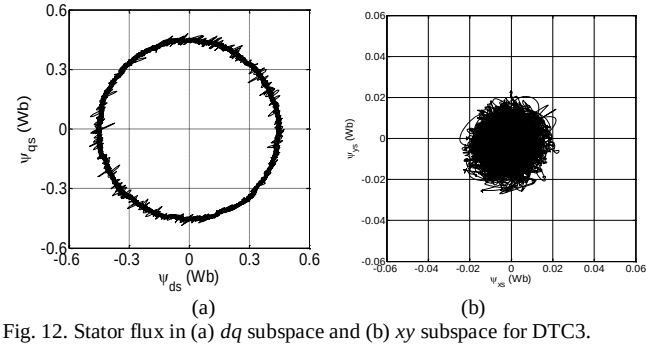

Fig. 12. Stator flux in (a) *dq* subspace and (b) *xy* subspace for DTC3.

as suggested in [12], [13], [16]. A three-level torque comparator is used in DTC1 and DTC2. However, the main benefit of the developed DTC3 method is that a five-level torque comparator can be used. This is obvious from Fig. 15c, which shows that a considerable reduction of torque ripple is achieved, when compared to the DTC1 and DTC2. Since the main difference between DTC1 and DTC2 relates to the control (or lack of it) of the *xy* voltage/current harmonics while the behaviour in the *dq* subspace is the same, these two techniques lead to essentially the same torque ripple, as shown with the numeric values in Table VI. The same table however shows that DTC3 substantially reduces the torque ripple value, to less than 40% of the value encountered with DTC1 and DTC2.

Variation of the torque ripple, as given with (9), with respect to the speed for three different loading conditions is compared in Fig. 16. DTC2 technique reduces only *xy* subspace harmonics, which do not affect torque response of the drive. It is clear from Fig. 16 that torque ripple for DTC1 and DTC2 is practically the same at different loading conditions and is significantly higher than the torque ripple obtained with the proposed DTC3 technique. Indeed, torque ripple is typically only 40% of the values obtained with DTC1 and DTC2. As can be seen in Table VI, this substantial reduction of the torque ripple is achieved with an insignificantly worsened phase current THD, when compared to the DTC2 (current THD of 12.1% for DTC2 against 12.9% for DTC3). Of course, DTC3 does significantly reduce the current THD when compared to DTC1 (current THD of 23.5%).

B. Dynamic Operation

Transient behaviour of the drive is compared for a change in speed reference and change in load torque. Dynamic performance for change in speed reference is shown in Fig. 17, where speed reference is stepped from 1000 rpm to 2000 rpm and dynamic variation of the electromagnetic torque and speed is recorded for the three discussed DTC techniques. It is inferred from Fig. 17 that the dynamic performance of the DTC3 scheme is essentially the same when compared to DTC1 and DTC2 methods. Disturbance rejection properties for a change in load torque are presented in Fig. 18. Initially the motor runs at 2000 rpm with a load of 0.3 Nm; the load torque is then increased from 0.3 to 2 Nm. It is observed from Fig. 18 that performance of the drive for change in the load torque with DTC3 remains just as good as with DTC1 and DTC2. Thus it is evident that the quality of the dynamic response of the drive is not affected by employing five-level torque comparator, used in DTC3.

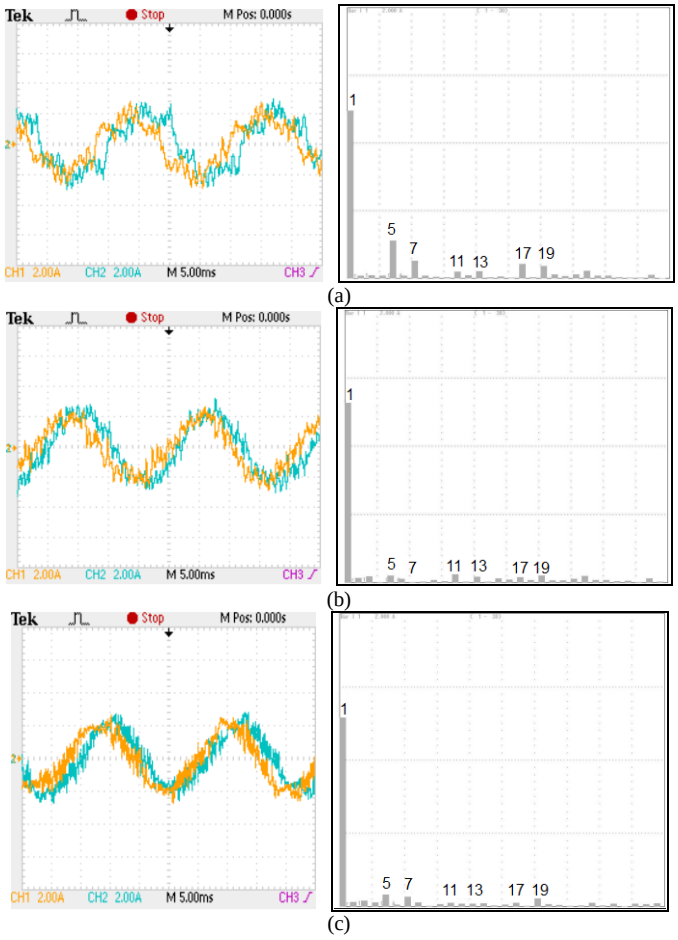

Fig. 13. Current of phases *a* and *b* (left, CH1: 2A/div, CH2: 2A/div, 5ms/div) and spectrum of phase *a* current (right) for: (a) DTC1, (b) DTC2, and (c) DTC3.

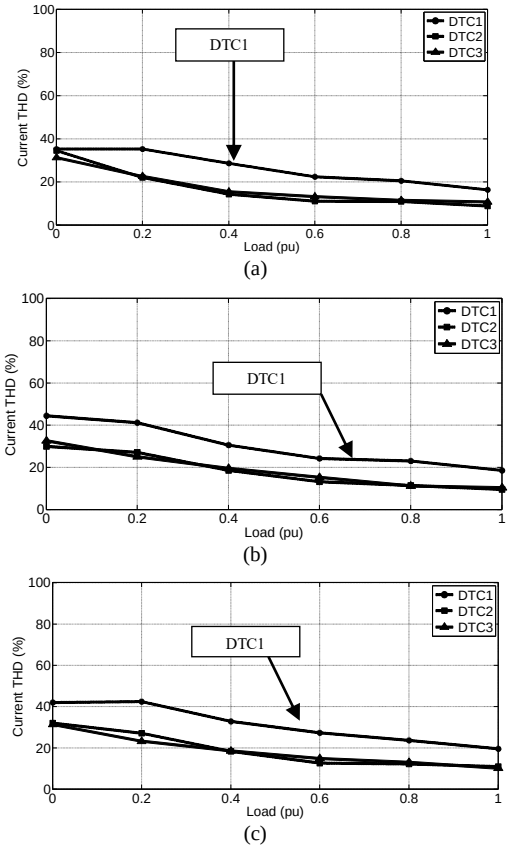

Fig. 14. Variation of stator current THD at (a) 500 rpm, (b) 1500 rpm, and (c) 2500 rpm.

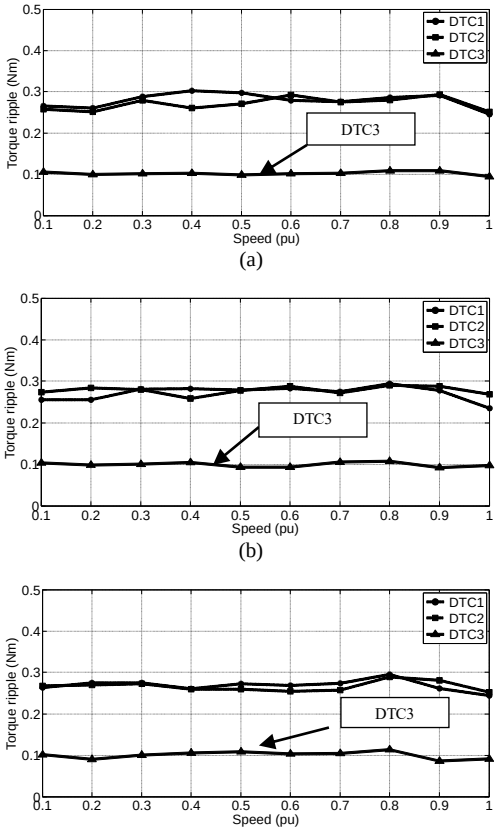

Fig. 16. Variation of torque ripple against per-unit speed at (a) no-load, (b) half-load, and (c) full load.

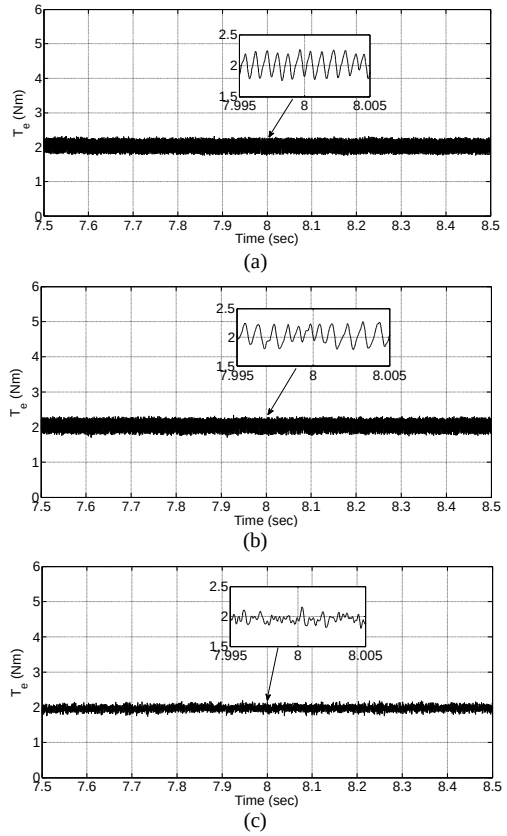

Fig. 15. Steady state torque waveform for (a) DTC1, (b) DTC2, and (c) DTC3 at 2500 rpm.

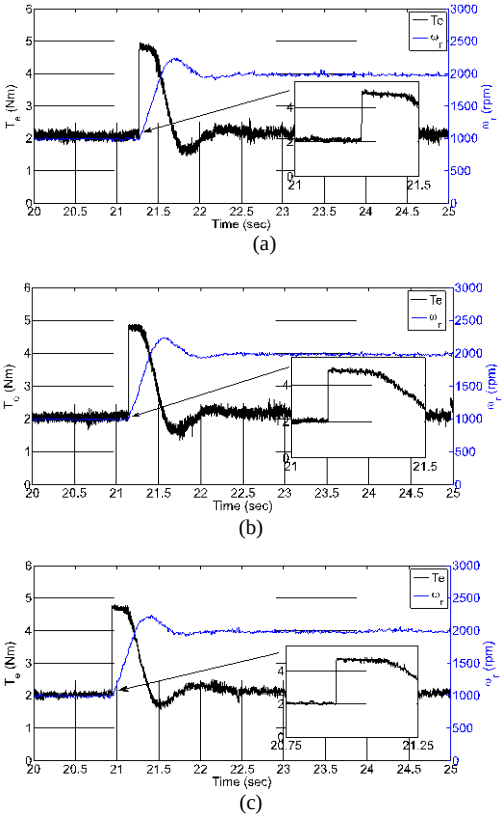

Fig. 17. Response of the drive to reference speed stepping from 1000 rpm to 2000 rpm: (a) DTC1, (b) DTC2, and (c) DTC3.

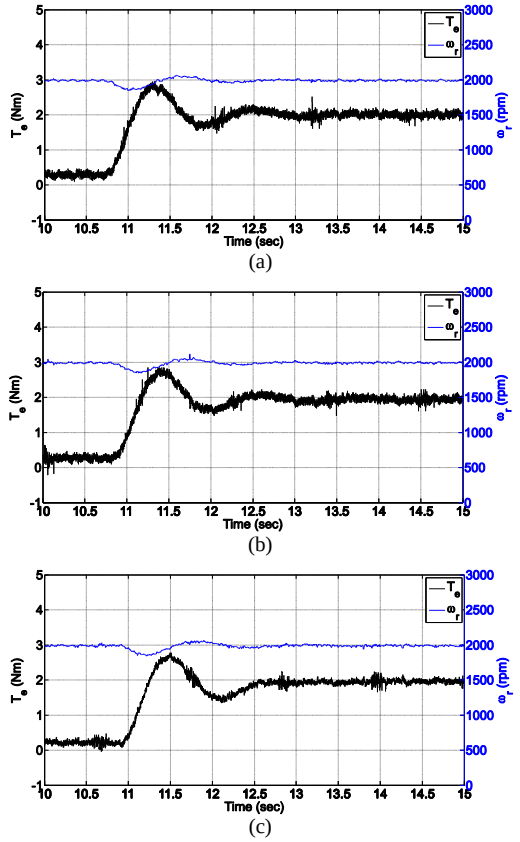

Fig. 18. Disturbance rejection behaviour of the drive, following a change in the load torque: (a) DTC1, (b) DTC2, and (c) DTC3.

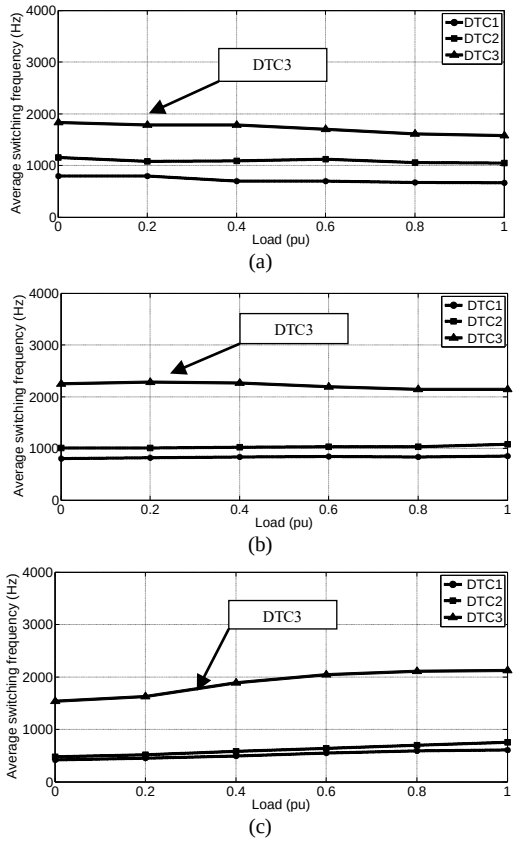

Fig. 19. Variation of average switching frequency against load at (a) 500 rpm, (b) 1500 rpm, (c) 2500 rpm.

TABLE VI. COMPARISON OF PERFORMANCE FOR DTC1, DTC2 AND DTC3.

Load = 2Nm; speed = 2500rpm	DTC1	DTC2	DTC3
Current THD (%)	23.5	12.1	12.9
Torque ripple (Nm)	0.2617	0.271	0.1063

C. Average Switching Frequency

As shown in Fig. 16 and Table VI, use of DTC3 leads to a significant reduction of the torque ripple. While this is of course advantageous, it is obtained at the expense of an increase in the average switching frequency. Fig. 19 illustrates behaviour of the average switching frequency, recorded experimentally for all three considered DTC techniques, against per unit load at three different operating speeds. As can be seen, average switching frequency of DTC1 and DTC2 is of a rather similar value for a given operating condition, with DTC2 having roughly 10% higher value. However, the average switching frequency with DTC3 is roughly double the value for DTC1. This is an expected outcome, since the DTC3 scheme presented here utilises small inverter vectors as well.

VII. CONCLUSION

Minimizing the negative effect of voltage vectors in the auxiliary (*xy*) subspace is necessary for any multiphase drive. An already available DTC technique (DTC2) is improved in the paper so that it generates two sets of virtual vectors, with the idea of subsequently improving the torque ripple behaviour by means of a five-level torque comparator. Virtual vectors are employed for the minimization of auxiliary (*xy*) subspace components and the implementation of the proposed DTC requires estimation of the flux position in the *xy* subspace. It is experimentally demonstrated that the quality of performance with regard to the stator current harmonics and THD remains at almost the same level as with DTC2 and is therefore significantly better than with DTC1. The subsequent use of the five-level torque comparator, which works in conjunction with two sets of virtual vectors, enables reduction of the torque ripple to around 40% of the value obtained in the other two DTC schemes. Importantly, the proposed DTC technique retains all the qualities of the other two DTC schemes, such as a simple structure and very good transient response, while operating with an increased average switching frequency. The technique is characterised with simple implementation requirements. Developments of the paper are verified by extensive experimentation.

REFERENCES

[1] E. Levi, R. Bojoi, F. Profumo, H. Toliyat, and S. Williamson, "Multiphase induction motor drives – a technology status review," *IET Electric Power Applications*, vol. 1, no. 4, pp. 489–516, July 2007.

[2] E. Levi, "Multiphase electric machines for variable-speed applications," *IEEE Transactions on Industrial Electronics*, vol. 55, no. 5, pp. 1893–1909, May 2008.

[3] F. Barrero and M. Duran, "Recent advances in the design, modeling, and control of multiphase machines part I," *IEEE Transactions on Industrial Electronics*, vol. 63, no. 1, pp. 449–458, Jan 2016.

[4] M. Duran and F. Barrero, "Recent advances in the design, modeling, and control of multiphase machines part II," *IEEE Transactions on Industrial Electronics*, vol. 63, no. 1, pp. 459–468, Jan 2016.

[5] E. Levi, "Advances in converter control and innovative exploitation of additional degrees of freedom for multiphase machines," *IEEE Transactions on Industrial Electronics*, vol. 63, no. 1, pp. 433–448, Jan 2016.

[6] K. Gopakumar, V. T. Ranganthan, and S. R. Bhat, "Split-phase induction motor operation from PWM voltage source inverter," *IEEE Transactions on Industry Applications*, vol. 29, no. 5, pp. 927–932, Sep 1993.
[7] Y. Zhao and T. Lipo, "Space vector PWM control of dual three-phase induction machine using vector space decomposition," *IEEE Transactions on, Industry Applications*, vol. 31, no. 5, pp. 1100–1109, Sep 1995.
[8] I. Takahashi and T. Noguchi, "A new quick-response and high-efficiency control strategy of an induction motor," *IEEE Transactions on Industry Applications*, vol. IA-22, no. 5, pp. 820–827, Sept 1986.
[9] M. Depenbrock, "Direct self-control (DSC) of inverter-fed induction machine," *IEEE Transactions on Power Electronics*, vol. 3, no. 4, pp. 420–429, Oct 1988.
[10] K. Hatua and V. Ranganathan, "Direct torque control schemes for split-phase induction machine," *IEEE Transactions on Industry Applications*, vol. 41, no. 5, pp. 1243–1254, Sept 2005.
[11] R. Bojoi, F. Farina, G. Griva, F. Profumo, and A. Tenconi, "Direct torque control for dual three-phase induction motor drives," *IEEE Transactions on Industry Applications*, vol. 41, no. 6, pp. 1627–1636, Nov 2005.
[12] K. D. Hoang, Y. Ren, Z.-Q. Zhu, and M. Foster, "Modified switching-table strategy for reduction of current harmonics in direct torque controlled dual-three-phase permanent magnet synchronous machine drives," *IET Electric Power Applications*, vol. 9, no. 1, pp. 10–19, 2015.
[13] Y. Ren and Z. Zhu, "Enhancement of steady-state performance in direct-torque-controlled dual three-phase permanent magnet synchronous machine drives with modified switching table," *IEEE Transactions on Industrial Electronics*, vol. 62, no. 6, pp. 3338–3350, June 2015.
[14] L. Zheng, J. Fletcher, B. Williams, and X. He, "A novel direct torque control scheme for a sensorless five-phase induction motor drive," *IEEE Transactions on Industrial Electronics*, vol. 58, no. 2, pp. 503–513, Feb 2011.
[15] L. Gao, J. Fletcher, and L. Zheng, "Low-speed control improvements for a two-level five-phase inverter-fed induction machine using classic direct torque control," *IEEE Transactions on Industrial Electronics*, vol. 58, no. 7, pp. 2744–2754, July 2011.
[16] Y. Ren and Z. Zhu, "Reduction of both harmonic current and torque ripple for dual three-phase permanent magnet synchronous machine using modified switching-table-based direct torque control," *IEEE Transactions on Industrial Electronics*, vol. 62, no. 11, pp. 6671–6683, Nov 2015.
[17] J.-K. Kang and S.-K. Sul, "New direct torque control of induction motor for minimum torque ripple and constant switching frequency," *IEEE Transactions on Industry Applications*, vol. 35, no. 5, pp. 1076–1082, Sep 1999.
[18] K.-B. Lee, J.-H. Song, I. Choy, and J.-Y. Yoo, "Torque ripple reduction in DTC of induction motor driven by three-level inverter with low switching frequency," *IEEE Transactions on Power Electronics*, vol. 17, no. 2, pp. 255–264, Mar 2002.
[19] A. Purcell and P. Acarnley, "Multilevel hysteresis comparator forms for direct torque control schemes," *Electronics Letters*, vol. 34, no. 6, pp. 601–603, Mar 1998.
[20] Z. Q. Zhu, Y. Ren, and J. Liu, "Improved torque regulator to reduce steady-state error of torque response for direct torque control of permanent magnet synchronous machine drives," *IET Electric Power Applications*, vol. 8, no. 3, pp. 108–116, March 2014.

Jay K. Pandit (S'16) received the B.E. degree in electrical engineering from Nagpur University, Nagpur, India, in 2009, and the M.Tech. degree in power electronics and drives from the Visvesvaraya National Institute of Technology, Nagpur, in 2014. From 2009 to 2012, he was an Operations Engineer with Reliance Infrastructure Ltd. His research interests include grid-connected inverters for distributed generation and electrical drives.

M. V. Aware (M'99, SM'14) received the B.E. degree in electrical engineering from the College of Engineering, Amravati, India, in 1980, the M.Tech. degree from the Indian Institute of Technology, Bombay, India, in 1982, and the PhD degree in 2002. From 1982 to 1989, he was a Design Officer with Crompton Greaves Ltd., Nasik, India and Development Engineer with Nippon Denso India Pvt. Ltd. From 1989 to 1991.

He is currently a Professor in the Department of Electrical Engineering, Visvesvaraya National Institute of Technology, Nagpur, India. His research interests include multi-phase electrical drives, distributed generation with energy storage and engineering application of fractional order calculus. He is a Fellow of the IE (India) and Fellow of the IETE (India). He is also certified energy auditor and a recipient of "Biman Bihari Sen" award from IETE (India) for 2016.

Ronak V. Nemade (S'16) received the B.E. degree in power electronics engineering from Gujarat Technological University, Ahmedabad, India, in 2013, and the M.Tech. degree in power electronics and drives from Visvesvaraya National Institute of Technology, Nagpur, India, in 2016. He is currently working with industrial electronics group at Central Electronics Engineering Research Institute, Pilani, India. His research interests include electric drives and power electronics converter topologies.

Emil Levi (S'89, M'92, SM'99, F'09) received his MSc and the PhD degrees in Electrical Engineering from the University of Belgrade, Yugoslavia in 1986 and 1990, respectively. From 1982 till 1992 he was with the Dept. of Elec. Engineering, University of Novi Sad. He joined Liverpool John Moores University, UK in May 1992 and is since September 2000 Professor of Electric Machines and Drives. He served as a Co-Editor-in-Chief of the IEEE Trans. on Industrial Electronics in the 2009-2013 period and is currently Editor-in-Chief of the IET Electric Power Applications and an Editor of the IEEE Trans. on Energy Conversion. He is the recipient of the Cyril Veinott award of the IEEE Power and Energy Society for 2009 and the Best Paper award of the IEEE Trans. on Industrial Electronics for 2008. In 2014 he received the "Outstanding Achievement Award" from the European Power Electronics (EPE) Association.